



# Long-Term Open-Path Dual-Comb Spectroscopy for Urban CO<sub>2</sub> Monitoring

Tobias D. Schmitt<sup>1</sup>, Romain Dubroeuq<sup>1,2</sup>, Moritz Sindram<sup>1,3</sup>, André Butz<sup>3,4,5</sup>, Thomas Pfeifer<sup>2</sup>, and Markus K. Oberthaler<sup>1</sup>

<sup>1</sup>Kirchhoff Institute for Physics (KIP), Heidelberg University, Germany

<sup>2</sup>Max Planck Institute for Nuclear Physics, Heidelberg, Germany

<sup>3</sup>Institute of Environmental Physics (IUP), Heidelberg University, Germany

<sup>4</sup>Heidelberg Center for the Environment (HCE), Heidelberg University, Germany

<sup>5</sup>Interdisciplinary Center for Scientific Computing (IWR), Heidelberg University, Germany

**Correspondence:** Tobias D. Schmitt([dcs\\_urban\\_co2@matterwave.de](mailto:dcs_urban_co2@matterwave.de))

**Abstract.** Accurate quantification of urban greenhouse gas (GHG) emissions can benefit from path-averaged, high-precision, high-temporal-resolution measurements that complement point sensors and passive remote sensing. Among open-path techniques, dual-comb spectroscopy (DCS) stands out as a particularly capable candidate, offering simultaneous broadband coverage, an absolute SI-traceable frequency axis, and sufficient spectral radiance for multi-kilometer paths. Here we present an open-path dual-comb spectrometer using two commercial, self-referenced, turn-key frequency combs operated continuously in Heidelberg, Germany, over an urban landscape. The instrument allows to infer column-averaged dry-air mole fractions of CO<sub>2</sub> along a 3.1 km absorption path. During routine observations within the evaluation period from September 2025 to February 2026 the system achieved a data coverage of 85%, with losses primarily attributable to visibility-limiting weather conditions such as fog and heavy rain. The instrument precision, characterized by the overlapping Allan deviation under stable atmospheric conditions, reaches  $4.79 \text{ ppm}\sqrt{\text{s}}$  for CO<sub>2</sub>, equivalent to 0.28 ppm at five minutes averaging time. These values are on par with or better than previous open-path DCS experiments and represent roughly one order of magnitude improvement over a co-deployed open-path Fourier transform spectrometer operating on the same path. The two instruments differ by a small bias of 0.16 ppm for CO<sub>2</sub>. The results demonstrate that high-quality, long-term open-path DCS operation is achievable with readily available hardware, making the technique accessible to the broader atmospheric science community for applications ranging from urban-flux monitoring and network-scale observations to the validation of spectroscopic databases.

## 1 Introduction

Carbon dioxide emissions from urban areas account for up to 70% of the global total, making urban emissions critical to climate change mitigation. Yet the urban emission landscape is inherently heterogeneous (Park et al., 2022; Hong et al., 2023), inducing large inventory uncertainties that typically increase with finer spatial and temporal resolutions (Gately and Hutyra, 2017; Oda et al., 2019; Super et al., 2020; Gurney et al., 2021). This heterogeneity also drives large spatial and temporal variability in urban CO<sub>2</sub> concentration fields (Zhu et al., 2022; Estruch et al., 2024; Mitchell et al., 2018). Atmospheric concentration

measurements can verify and improve emission inventories from a top-down perspective (Lauvaux et al., 2020; Mueller et al., 2021). However, the heterogeneity poses a significant challenge to models and measurements, which must either resolve or correctly average the induced variability, while being sensitive to urban emissions.

25 Point sensors provide local atmospheric CO<sub>2</sub> records but suffer from representativeness bias at urban scales due to spatial heterogeneity (e.g., Kaminski et al., 2001). Vertical column measurements from satellites and ground-based sun-viewing spectrometers lack sensitivity to local urban emissions and suffer from limited temporal coverage due to weather conditions and daytime-only availability. In contrast, open-path measurements that average over kilometer-scale horizontal paths provide representativeness at typical model grid scales while maintaining sufficient sensitivity to detect urban emissions. Open-path  
30 techniques may also serve as calibration references for emerging dense low-cost sensor networks (e.g., Shusterman et al., 2016; Kim et al., 2025; Asimow et al., 2025; Patel et al., 2026).

The core difficulty of open-path CO<sub>2</sub> measurements lies in detecting small relative signals (~1 ppm enhancements against ~420 ppm background abundance). In the near-infrared, this difficulty is compounded by intrinsically weak absorption. This combination of small relative signal and weak absorption demands spectrometers with high signal-to-noise ratio. Multiple  
35 technological approaches have been explored for kilometer-scale open-path CO<sub>2</sub> measurements. Early techniques adapted differential optical absorption spectroscopy (DOAS), originally developed in the visible and ultraviolet, to the near-infrared using grating spectrometers paired with thermal light sources (e.g., Saito et al., 2015). Open-path Fourier transform infrared (FTIR) spectrometers later improved upon this approach, achieving broader spectral coverage and enabling simultaneous retrieval of multiple species (Griffith et al., 2018; Deutscher et al., 2021; Schmitt et al., 2023). Both approaches, however, are fundamen-  
40 tally constrained by the limited spectral radiance of thermal sources, which severely restricts achievable signal-to-noise ratio. Consequently, both suffer from limited precision, typically achieving only a few ppm on minute timescales. Furthermore, their limited spectral resolution introduces accuracy problems due to instrument line shape effects.

Laser-based approaches can overcome these limitations and achieve high sensitivity and high spectral resolution at the same time. The simplest laser-based approach uses on-band-off-band measurements, meaning two fixed-wavelength lasers with one  
45 tuned to a CO<sub>2</sub> absorption line and one offset. It was the first method deployed at scale for urban emissions inference (Dobler et al., 2013, 2017; Lian et al., 2019). However, this approach suffers from temperature-dependent biases of tens of ppm, especially when the lasers are not actively stabilized to the absorption feature (Zaccheo et al., 2019).

Tunable diode laser absorption spectrometers (TDLAS) improve upon this approach by measuring across full absorption features, enhancing stability to changes in environmental conditions. Nevertheless, TDLAS faces fundamental limitations:  
50 temperature-concentration degeneracy and insufficient spectral information to resolve interfering species complicate the retrieval of unambiguous CO<sub>2</sub> column amounts (Plant et al., 2015; Bailey et al., 2017). Broad spectral coverage spanning multiple ro-vibrational bands is required to resolve these limitations and simultaneously measure multiple interfering species.

Dual-comb spectroscopy (DCS, e.g., Coddington et al., 2016; Picqué and Hänsch, 2019) is a natural candidate for filling this role (Cossel et al., 2021). It offers simultaneous broadband spectral coverage enabling multi-species detection in a single mea-  
55 surement; an absolute, SI-traceable frequency axis that requires no wavelength calibration and provides direct spectroscopic accuracy; and high spatial coherence that maintains adequate signal-to-noise ratios over multi-kilometer paths even with  $\mu$ W-



level return signals. The first open-path DCS demonstration for atmospheric GHG sensing was reported by Rieker et al. (2014), followed by a quantitative intercomparison (Waxman et al., 2017) and the first applications to emission quantification in urban (Waxman et al., 2019) and agricultural (Herman et al., 2021) settings. Giorgetta et al. (2021) demonstrated open-path DCS operation in the mid infrared. Most recently, a DCS open-path system was deployed near the background station at Mauna Loa Observatory in an attempt to verify cross-section databases, leveraging the superior accuracy DCS can achieve relative to other open-path methods (Malarich et al., 2025). All of these advances originated from NIST, Boulder, Colorado, and collaborating institutions.

Building on this foundation, open-path DCS was commercialized for methane detection in oil and gas infrastructure (Coburn et al., 2018; Alden et al., 2019, 2020; Mead et al., 2023), with systems deployed for continuous monitoring. However, these commercial deployments remain focused on a single analyte (methane) and a specialized application domain, and the technology has remained within the expertise ecosystem of its original developers.

In parallel, alternative approaches such as drone-based reflectors (Cossel et al., 2017, 2023) or open-path DCS sensing in the ultra-violet (Eber et al., 2024), have also been explored. Further, Han et al. (2024) demonstrated DCS operation over distances exceeding 100 km. While many of these DCS deployments were based on custom-built hardware and operation required a high level of metrology expertise, the recent maturation of commercial, self-referenced, turn-key frequency comb systems (e.g., Quatrevalet et al., 2025) and the here reported results take DCS usage closer to routine use within the atmospheric measurement community.

Here we present an open-path dual-comb spectrometer using commercial, turn-key, self-referenced combs, operating over a 3.1 km urban path in Heidelberg, Germany. The system measures column-averaged dry-air mole fractions of  $\text{CO}_2$  ( $x\text{CO}_2$ ) and  $\text{CH}_4$  ( $x\text{CH}_4$ ) simultaneously and continuously. We validate its performance through comparison with a co-located FTIR that operates along the same light path (Schmitt et al., 2023). The remainder of this paper is structured as follows: Section 2 describes the experimental setup; Section 3 details the data evaluation and spectral retrieval; Section 4 presents results and validation.

## 2 Dual-Comb setup

Two frequency combs (SmartCombs from MenloSystems) with a comb mode spacing of 100 MHz and a central wavelength of about 1560 nm at a full-width-half-maximum of 30 nm (45 nm for the second comb) form the core of the spectrometer. The lasers provide five outputs at 5 mW each, and one output which is amplified and then broadened in a highly nonlinear fiber (HNLF), with a total output power up to 100 mW and a spectral coverage spanning up to an octave from 1 to 2  $\mu\text{m}$ . Further, the lasers are self-referenced, turn-key systems, which provide a radio-frequency-lock of the repetition rate  $f_{rep}$  and offset frequency  $f_{ceo}$  to either an internal or external 10 MHz reference out of the box. Both combs are then referenced to an external 10 MHz Rubidium clock (FE-5680A, FEI Communications). Locking the repetition rate of each comb to a common external optical reference improves the mutual coherence of the two combs. To this end, our combs are also configured with a beat detection unit (BDU) at 1542.14 nm, which accepts an optical reference at the correct wavelength via a fiber port. Our external

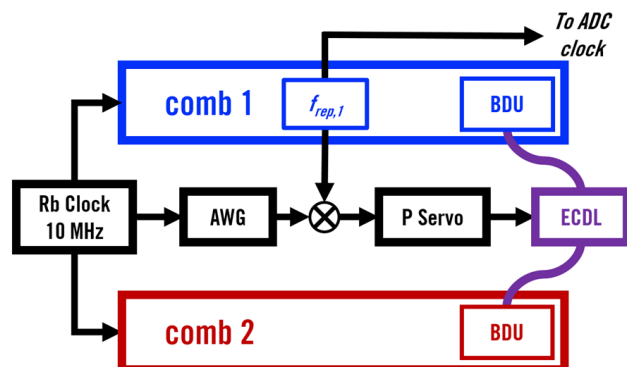


**Figure 1.** Locking scheme of the dual comb setup. The blue and red boxes indicate the SmartCombs and their internal modules. Black lines are electronic connections, colored lines optical fibers. The CEO of each comb is radio-frequency locked to a mutual 10 MHz frequency standard, provided by a Rubidium clock. The RRs are locked to an optical reference, an ECDL at 1542.14 nm, via a beat detection unit (BDU) within the comb package. To compensate for long term drifts the RR of comb 1 is locked to exactly 100 MHz by slowly acting on the ECDL.

90 reference laser is a continuous-wave narrow-linewidth (<100 Hz) external cavity diode laser (ECDL) from NKT Photonics (Koheras Basik X15). The internal frequency counter of the frequency combs measure the  $f_{ceo}$  and  $f_{rep}$  frequencies, as well as the beat-note to the reference laser in 1s intervals. This enables the reconstruction of the frequency axis with respect to the Rubidium clock.

Figure 1 shows the complete locking scheme, with the two frequency combs indicated by the blue and red boxes. Both 95 combs are referenced to the Rubidium clock and locked to the external ECDL reference via their BDU. The offset frequencies of both combs are stabilized to the 10 MHz reference (not represented in the figure). A bootstrapped approach is used to further stabilize the system (e.g., Truong et al., 2016): the first comb's  $f_{rep}$  is actively locked to exactly 100 MHz through feedback on the ECDL frequency. The lock error signal is generated by mixing  $f_{rep}$  with a reference signal from an arbitrary waveform generator (AWG, Siglent SDG6022X), referenced to the 10 MHz clock. The mixer output is low-pass filtered and fed to a 100 digital servo controller (DCS1, Thorlabs) with proportional-only gain, whose output drives the ECDL frequency control. This feedback loop, combined with the internal integration in the reference laser module, stabilizes both the ECDL frequency and the locked repetition rates over extended timescales, eliminating long term drifts and allowing averaging times of minutes or longer.

We employ a DCS scheme where we overlap the two frequency combs HNLFF outputs in free-space using a wedged 50:50 105 non-polarizing beam-splitter (BSW18, Thorlabs), before we transmit the light through the atmosphere. The beam-splitter may be replaced by a  $2 \times 2$  50:50 fiber coupler (PN1550R5A2, Thorlabs) for a more compact setup, but at the cost of a narrower spectral bandwidth. Either fiber or free-space coupler induce a 3 dB loss on the input power, due to the use of a non-polarizing beam-splitter. Currently we use the second output of the beam-splitter to monitor the spectral envelope with a grating spectrometer (waveScan Extended IR spectrometer, APE), but in principle it can supply a second light path of the open-path system.

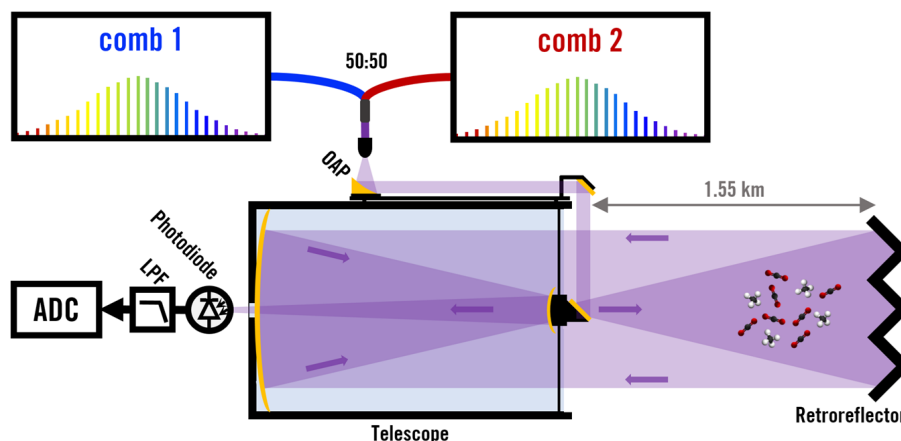


**Figure 2.** Open path DCS setup. After mixing the light of the two frequency combs, it is launched to an array of retro reflectors. A larger, co-aligned telescope collects the return light and images it on a detector. The electrical signal is filtered, digitized, averaged and transmitted to a PC for long term averaging and further analysis. OAP, off-axis parabolic mirror; LPF, low-pass filter, ADC, analog-to-digital converter.

110 Figure 2 sketches the transceiver setup for the atmospheric open-path measurements: The employed design consists of a smaller transmitting telescope concentric within a larger receiving telescope. The transmitting telescope does not cause additional obstruction of the return light, since it is smaller than the secondary mirror of the receiving telescope (GSO 8" Ritchey-Chretien Pro 203/1624 mm, TS-Optics). The main optic of the transmitting telescope is a 50.8 mm off-axis parabolic mirror with a focal length of 190.5 mm, which is mounted on top of the tube of the receiving telescope to form a compact

115 package. The receiving telescope images directly onto the detector (PDA05CF2, Thorlabs). This transceiver telescope package accepts a fiber input of the already mixed dual-comb light and outputs the electronic signal from the detector. We initially tested telescope designs using a shared main mirror with a beam-splitter to separate transmit and receive paths. This design suffered from additional etalons and multi-reflections in the beam-splitter, resulting in substantial signal contamination from light that never traveled the atmospheric path. This is consistent with the observations by Waxman et al. (2017). The reflector array is

120 currently the same as in Schmitt et al. (2023) and consists of solid glass cube-corners relying on total internal reflection. Their reflectivity is in the range of 70% at 1.6  $\mu\text{m}$  and the array has a geometric loss of roughly 50% due to the spacing and housing of the circular reflector modules. In total we receive on average about 55  $\mu\text{W}$  of the 7.2 mW launched by the telescope, putting the total system transmission at 0.8%. This is comparable to the results by Waxman et al. (2017).

The electronic signal is low-pass filtered (SLP-44+, Mini-Circuits) to ensure it stays below our Nyquist limit of 50 MHz, and

125 attenuated (-3dB) to reliably match the dynamic range of our analog-to-digital converter (ADC). We digitize the signal using a RedPitaya board (SDRlab 122-16 External Clock, RedPitaya), which includes an onboard ADC and an input for an external clock. We provide a 100 MHz clock signal, which we derive from the first frequency comb's  $f_{rep}$ , to ensure synchronized sampling. In a first step we acquire one second of data with deep memory acquisition directly into the RAM of the RedPitaya, using the available high level Python API. Next, we locate the individual interferograms (IFGs) and add them up, overlapping



**Table 1.** List of equipment.

type of equipment	model	manufacturer
frequency combs	SmartCombs	MenloSystems
reference laser	Koheras Basik X15	NKT Photonics
Rubidium clock	FE-5680A	FEI Communications
function generator	SDG6022X	Siglent
servo controller	DSC1	Thorlabs
non polarizing beam-splitter	BSW18	Thorlabs
grating spectrometer	waveScan Extended IR spectrometer	APE
return telescope	GSO 8" Ritchey-Chretien Pro 203/1624 mm	TS-Optics
off-axis parabolic mirror	50.8 × 190.5mm EFL 90° Protected Gold	Edmund Optics
detector	PDA05CF2	Thorlabs
acquisition system	SDRlab 122-16 External Clock	RedPitaya
pressure sensor	PTB330 (A0AAHAACEB0A0B)	Vaisala

130 and centering them at the maximum point of the IFG. This rudimentary averaging algorithm is enabled by the high mutual coherence of the two combs from the active stabilization of their parameters relative to the reference laser.

After averaging these one second intervals on the RedPitaya, we transfer the averaged IFG via an ethernet connection to a PC, where we average them further to match the desired time resolution. The whole process of acquiring the one second of data, averaging it and sending it to the PC takes about 4.2 seconds. As a result our duty cycle is around 24%, i.e. a factor of 1/2  
 135 in SNR. In the future, the implementation of real-time averaging at the hardware level will allow us to recover this factor.

Finally, we also collect auxiliary data, which we need to process the measured spectra. For temperature measurements, we use either the information provided by a local meteorological weather station or auxiliary output from our pressure sensor. The exact source is not critical, since the path-averaged temperature is fitted in the retrieval (see Sect. 3 for details) and only requires a reasonable first guess. The most relevant environmental parameter is pressure, since it impacts the later retrieved mole  
 140 fractions linearly. While we can fit pressure from our spectra, doing so results in a worse constraint of the target gas species ( $x\text{CO}_2$  precision decreases by 0.3 ppm for 1 min measurements) and in a quite uncertain pressure value (4 hPa uncertainty for 1 min measurements). Thus, we measure pressure using a PTB330-A sensor (from Vaisala), which is accurate to  $\sim 0.1$  hPa, and corrected for average path height above the sensor (4.5 m).

After receiving the frequency combs in mid-September 2024, the system is operational in the presented configuration since  
 145 early August 2025. After running multiple tests in August and improving our data storage strategy, we acquired the dataset shown in this work, starting 02 September 2025. Table 1 gives a full list of the above mentioned equipment making up our open-path DCS observatory.

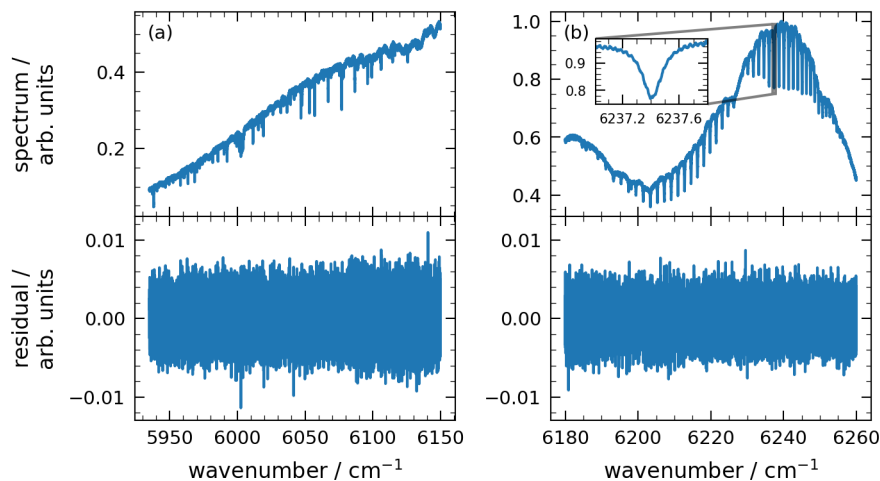


**Figure 3.** One minute absorption spectrum and corresponding fit residual along the open path of 3106 m total length. Measured on 30 October 2025, 14:27 UTC. Spectral sampling of  $3.34 \times 10^{-3} \text{ cm}^{-1}$ . Panel (a):  $\text{CH}_4$  evaluation window. Panel (b):  $\text{CO}_2$  evaluation window, including a zoom into a single absorption line.

### 3 Data evaluation

To retrieve trace gas information from the measurements, we Fourier transform the IFGs and reconstruct the optical frequency axis from recorded comb parameters. The result is a spectrum as depicted in Fig. 3. We fit the baseline using a cepstral approach (Cole et al., 2019), implemented similar to Malarich et al. (2025). In each optimization step, we treat the residual of all times below 38 ps, which also includes the main etalon of the lab window, as contribution of the baseline. We further include narrow regions from 793 ps to 800 ps, 880 ps to 895 ps, and 899 ps to 906 ps in this baseline treatment, since these regions contain spurious noise which likely results from the lasers themselves. Otherwise, the spectral fit contains only Beer-Lambert's law and is derived from the algorithm described in Schmitt et al. (2023), but adapted and improved for higher spectral resolution and faster runtime.

We compute absorption cross-sections for  $\text{CH}_4$  via the HAPI interface (Kochanov et al., 2016), using speed-dependent Voigt (SDV) parameters from HITRAN2024 (Gordon et al., 2026), including the available line-mixing and water-vapor broadening parameters. For  $\text{CO}_2$ , we follow the recent HITRAN recommendation (Gordon et al., 2026, page 12) and use the results from Birk et al. (2024a) (dataset: Birk et al., 2024b), which include pressure depletion and continuum absorption, as well as water-vapor broadening, all from the same set of measurements. Their published pre-computed absorption-cross-section database (Birk et al., 2025) also contains information on interfering  $\text{H}_2\text{O}$  lines, which we use where available, defaulting to HITRAN2024 where not. We use a modified version of this data product on a different temperature and pressure grid, to better fit our parameter space of lower troposphere conditions, which we received through private communications. We use the HITRAN standard mixture of isotopologues for all three species ( $\text{CO}_2$ ,  $\text{CH}_4$ , and  $\text{H}_2\text{O}$ ).

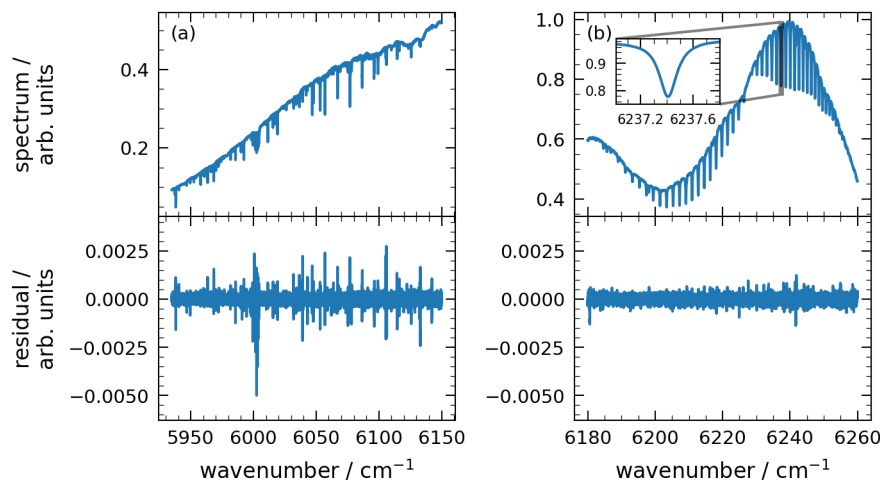


**Figure 4.** Absorption spectrum averaged over eight hours and corresponding systematic fit residual along the open path of 3106 m total length. Measured on 30 October 2025, from 08:30 to 16:30 UTC. Spectral sampling of  $3.34 \times 10^{-3} \text{ cm}^{-1}$ . The stronger systematic residuals for the CH<sub>4</sub> evaluation window (a) are clearly visible in comparison to the CO<sub>2</sub> evaluation window (b).

We fit individual spectra averaged over a duration of one minute, using pressure information on one end of the path and correcting it for the average height of the path above the sensor position (4.5 m). We use locally measured temperature as an initial guess, but fit a path averaged temperature from the spectrum. We split the spectrum in two evaluation windows (Fig. 3): one from  $5935 \text{ cm}^{-1}$  to  $6150 \text{ cm}^{-1}$ , which we call the CH<sub>4</sub> window, and one from  $6180 \text{ cm}^{-1}$  to  $6260 \text{ cm}^{-1}$ , which we call the CO<sub>2</sub> window, both after the main absorbers in the respective spectral ranges. Finally, we convert the fitted total absorber columns to dry-air mole-fractions by using the measured pressure, the fitted path-averaged temperature, and the fitted water column to calculate the dry-air column.

In both windows, the residuals are dominated by statistical noise for averaging times of one minute, as Fig. 3 illustrates. The noise level is typically below 1% of the maximal signal intensity and mostly independent of the signal strength, as the constant noise band over both evaluation windows shows. This is expected from a system mostly limited by detector-noise. Averaging consecutive residuals over eight hours reveals a systematic residual which shows substantial differences for the two windows (Fig. 4). In the CO<sub>2</sub> window, the residual is still partially defined by random noise together with a few clear line residuals, e.g., the strongest one at  $6241.7 \text{ cm}^{-1}$ , which we could attribute to water lines. However, this is different for the CH<sub>4</sub> window, where the systematic residual is visibly dominated by several structures associated with absorption features. H<sub>2</sub>O lines and CH<sub>4</sub> line-clusters show strong systematic features in the fit residual. This illustrates the substantial recent improvements to the spectroscopic description of the respective CO<sub>2</sub> absorption-bands, as well as the challenge that the accurate description of CH<sub>4</sub> still poses. The CH<sub>4</sub> spectroscopic information remains under active development, with updates covering only subsets of absorption lines, making the retrieval substantially more complex than for CO<sub>2</sub>. We therefore focus in the following analysis on CO<sub>2</sub> to clearly demonstrate the system's capabilities, deferring comprehensive CH<sub>4</sub> characterization to future work.

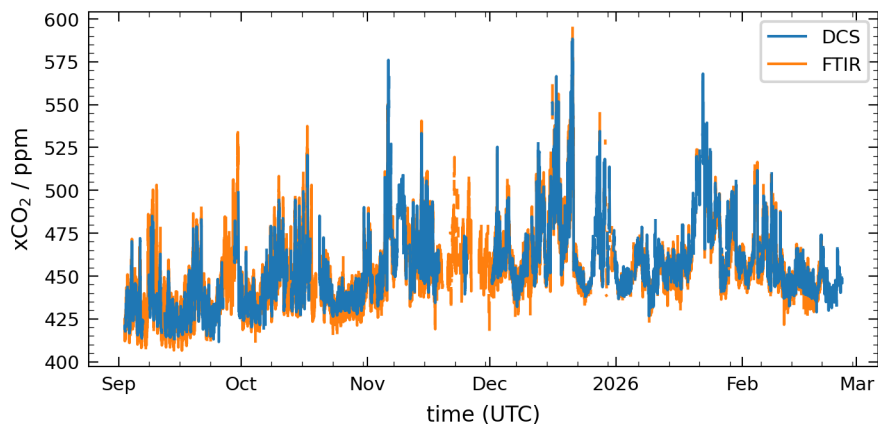


**Figure 5.** Time-series of  $x\text{CO}_2$  for the DCS instrument (this work) and a co-deployed FTIR instrument (Schmitt et al., 2023) for the full reported period. Time resolution of 5 minutes.

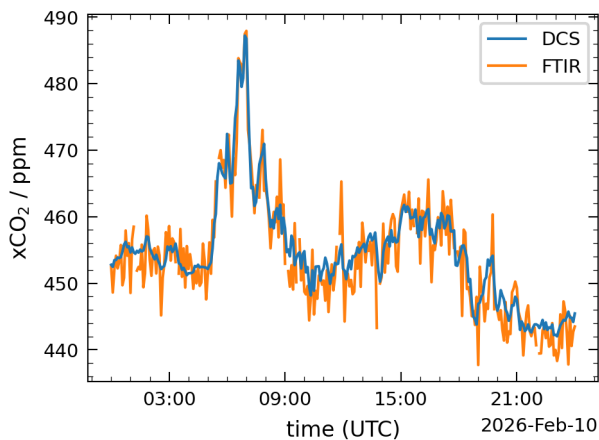


**Figure 6.** Time-series of  $x\text{CO}_2$  for the DCS instrument (this work) and a co-deployed FTIR instrument (Schmitt et al., 2023) for 24 hours. Time resolution of 5 minutes.

## 185 4 Results

The evaluation period spans from 02 September 2025 to 25 February 2026. Figure 5 shows the retrieved dry-air mole fraction of  $\text{CO}_2$  ( $x\text{CO}_2$ ) for the DCS open-path instrument in comparison with a FTIR open-path instrument (Schmitt et al., 2023). To address the different acquisition times of individual measurements for each instrument, the measurements are binned and averaged on a time grid of 5 minutes. The DCS instrument demonstrates a coverage of 76% of the 5 minute bins, after filtering  
190 the DCS data for measurements of extremely low signal of less than 5%, typically resulting from strong rain or fog, and

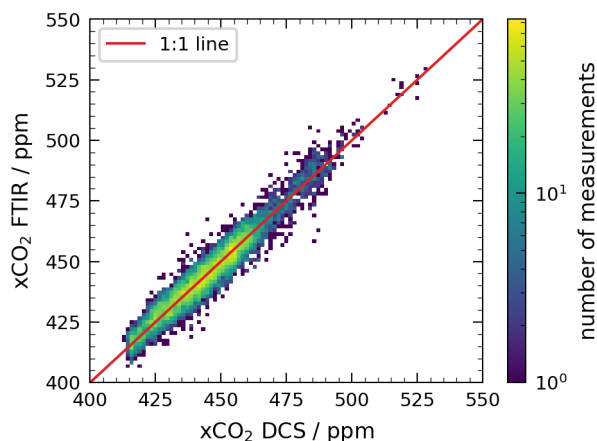


**Figure 7.** Correlation of  $x\text{CO}_2$  measurements between the two instruments in a 2D-histogram. A simple fit reveals a high bias of 0.16 ppm for the FTIR instrument.

conservatively for unexpectedly high  $\chi_{\text{red}}^2$  of the spectral fit. The two major data gaps from mid to end of November result from benchmarking tests for different modes of operation, which are not covered here. In the following, the system shows up times of about 85%. Both instruments show the same long-term trends like the typical annual cycle of increased  $\text{CO}_2$  in the northern-hemisphere winter and agree well along the full time-series. While the better precision of the DCS system over the FTIR is already visible on this time scale, it becomes substantially clearer when zooming into a single day (Fig. 6). Both instruments are in good agreement within their respective precision throughout the day, where the diurnal cycle is dominated by boundary layer dynamics, with the FTIR instrument showing a substantially higher scatter. This reduced scatter in the DCS measurements makes it substantially easier to discern actual temporal variations of the  $\text{CO}_2$  concentration from measurement noise compared to the FTIR data.

The correlation of the  $x\text{CO}_2$  values between the two instruments is close to a one-to-one line as Fig. 7 shows, further attesting to the good performance of both open-path spectrometers. A fit reveals only a minimal bias of 0.16 ppm between them, with the FTIR high-biased versus the DCS instrument.

Finally, we quantify the performance of the instrument by calculating the overlapping Allan deviation for 400 consecutive data-points, measured 12 September 2025 from 10:04:12 UTC to 16:16:26 UTC, during relatively stable atmospheric conditions. Figure 8 shows the expected  $\tau^{-1/2}$  scaling for averaging times  $\tau$  below approximately 400 s, where atmospheric variability starts to dominate the measurement uncertainty. From fitting a function of type  $a \cdot \tau^{-1/2}$  to the first seven data-points, we determine the instrument performance from the proportionality factor  $a$  to  $4.79 \text{ ppm}\sqrt{\text{s}}$ . This is equivalent to a precision of 0.28 ppm at an averaging time of five minutes for the DCS instrument, outperforming the FTIR instrument by an order of magnitude (2.7 ppm, Schmitt et al., 2023). Figure 8 also shows, that the performance compares well to previous DCS open-path experiments, outperforming all but Waxman et al. (2019) in its current state, and even improving on that as soon as the implementation of real time averaging improves the performance at least by another factor of two.

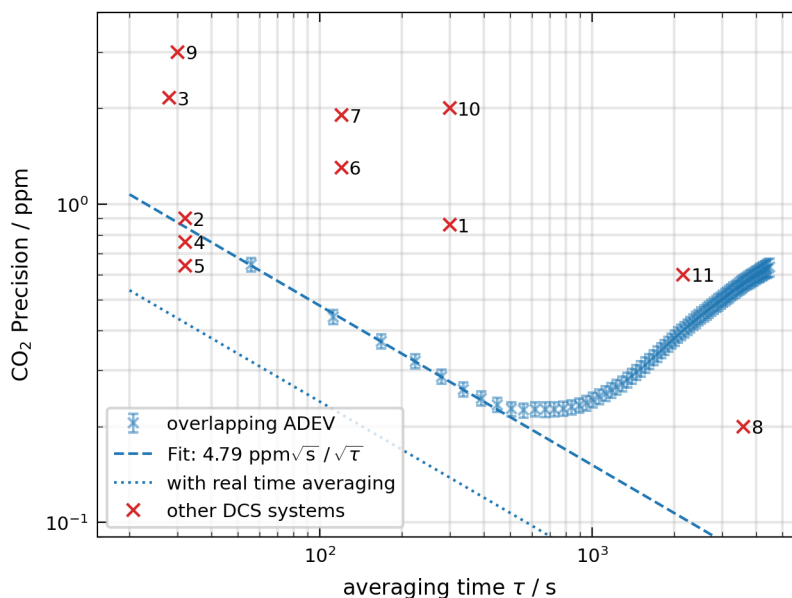


**Figure 8.** Overlapping Allan deviation for DCS  $x\text{CO}_2$  measurements. The time between individual data-points of original time-series is 45 s. The fit shows the expected  $\tau^{-1/2}$  scaling of gaussian noise for low averaging times, where the measurement noise dominates the real atmospheric variability. The dashed line corresponds to the same performance extrapolated under the assumption of real time averaging. Previously reported precisions are marked in the plot for reference and numbered. The corresponding references are: (1) Rieker et al. (2014), (2) DCS A of Waxman et al. (2017), (3) DCS B of Waxman et al. (2017), (4) 2 km path of Waxman et al. (2019), (5) 6.7 km path of Waxman et al. (2019), (6) 0.6 km path of Giorgetta et al. (2021), (7) 2 km path of Giorgetta et al. (2021), (8) Malarich et al. (2025), (9) Chen et al. (2023), (10) Han et al. (2024) at 5 min averaging time, (11) Han et al. (2024) at 1 h averaging time,

Performing a similar analysis for  $\text{CH}_4$ , yields a precision of  $52 \text{ ppb}\sqrt{s}$  or 3.0 ppb for averaging time of five minutes, again comparing well to Waxman et al. (2017), with their reported values corresponding to  $54 \text{ ppb}\sqrt{s}$  and  $61 \text{ ppb}\sqrt{s}$ , as well as providing a substantial improvement over the FTIR instrument (18 ppb at 5 min, Schmitt et al., 2023).

## 215 5 Conclusions

We presented an open-path dual-comb spectrometer using exclusively commercial, turn-key, self-referenced combs. It allows to retrieve column-averaged dry-air mole fractions of  $\text{CO}_2$  and  $\text{CH}_4$  over a 3.1 km urban path in Heidelberg, Germany. Over the evaluation period from 02 September 2025 to 25 February 2026, the instrument achieved a data coverage of 76%, with uptime of approximately 85% during committed routine observations; data losses were primarily attributable to visibility-limiting  
220 weather conditions such as fog and heavy rain. The DCS instrument reaches a  $\text{CO}_2$  precision of  $4.79 \text{ ppm}\sqrt{s}$ , corresponding to



0.28 ppm at five minutes averaging time. This is on par with or better than previous open-path DCS experiments and represent roughly one order of magnitude improvement over the co-deployed open-path FTIR instrument (Schmitt et al., 2023).

Direct comparison between the DCS and FTIR instruments reveals excellent agreement, with only 0.16 ppm bias in  $x\text{CO}_2$  between the two instruments. Systematic fit residuals in the  $\text{CO}_2$  evaluation window are small and partially attributable to  
225 known water-vapor absorption lines, confirming the maturity of current spectroscopic databases for this region (Birk et al., 2024a). By contrast, systematic residuals in the  $\text{CH}_4$  window remain substantial, reflecting ongoing challenges in spectroscopic description; comprehensive characterization of the  $\text{CH}_4$  retrieval is left for future work.

The DCS system operates in the vicinity of a dense sensor network currently being deployed in Heidelberg, enabling three complementary scientific contributions: (1) characterization of sensor biases and drift through direct comparison with  
230 high-quality reference measurements; (2) gradient-based constraints on urban emissions through path-averaged measurements, which can complement or validate emission estimates derived from in-situ networks; and (3) combined interpretation of dense in-situ and path-averaged data to disentangle spatial heterogeneity in urban  $\text{CO}_2$  from measurement artifacts.

Beyond applications within the local metropolitan area, the high spectral resolution and signal-to-noise ratio make the DCS instrument valuable for validating absorption cross-section databases, addressing ongoing questions about, e.g., continuum  
235 absorption and water-vapor broadening parameterization of  $\text{CO}_2$  (Birk et al., 2024a; Malarich et al., 2025).

This work demonstrates that the maturation of commercial frequency-comb technology has fundamentally transformed open-path DCS from a specialized metrology technique into an accessible tool for the broader atmospheric science community. These advances establish a foundation for distributed, high-quality atmospheric observations spanning greenhouse gas monitoring and beyond, enabling diverse sensing solutions and broader applications in atmospheric chemistry and air quality  
240 assessment.

*Code and data availability.* Code and Data are available from the authors upon request.

*Author contributions.* All authors conceived and designed the instrument and contributed to the writing of the paper. TDS, RD and MS developed the instrument. TDS and MS carried out the formal data analysis. TDS prepared the manuscript.

*Competing interests.* At least one of the Authors is a member of the editorial board of Atmospheric Measurement Techniques.

245 *Acknowledgements.* The authors want to express gratitude to Ian Coddington, Nathalie Picqué, Birgitta Schultze-Bernhardt and her team, and Marcus Ossiander for the valuable scientific exchange at the beginning of this project. Many thanks go to Manfred Birk and Georg Wagner for providing their absorption-crosssection database on a custom grid. The authors gratefully acknowledge the data storage service SDS@hd supported by the Ministry of Science, Research and the Arts Baden-Württemberg (MWK) and the German Research Foundation

<https://doi.org/10.5194/egusphere-2026-2428>

Preprint. Discussion started: 8 May 2026

© Author(s) 2026. CC BY 4.0 License.



250 (DFG) through grant INST 35/1503-1 FUGG. The authors acknowledge support by the state of Baden-Württemberg through bwHPC and the DFG through grant INST 35/1597-1 FUGG. The Instrument was funded by the state of Baden-Württemberg and the DFG through grant INST 35/1790-1 FUGG. The authors utilized artificial intelligence tools in the generation of portions of manuscript text and figures. The authors take full responsibility for the accuracy and integrity of all content.



## References

- Alden, C. B., Coburn, S. C., Wright, R. J., Baumann, E., Cossel, K., Perez, E., Hoenig, E., Prasad, K., Coddington, I., and Rieker, G. B.:  
255 Single-Blind Quantification of Natural Gas Leaks from 1 Km Distance Using Frequency Combs, *Environ. Sci. Technol.*, 53, 2908–2917,  
<https://doi.org/10.1021/acs.est.8b06259>, 2019.
- Alden, C. B., Wright, R. J., Coburn, S. C., Caputi, D., Wendland, G., Rybchuk, A., Conley, S., Faloon, I., and Rieker, G. B.: Temporal  
Variability of Emissions Revealed by Continuous, Long-Term Monitoring of an Underground Natural Gas Storage Facility, *Environ. Sci.*  
*Technol.*, 54, 14 589–14 597, <https://doi.org/10.1021/acs.est.0c03175>, 2020.
- 260 Asimow, N. G., Patel, M. Y., Zhu, Y., Winter, A. R., Gurney, K. R., Berelson, W. M., Turner, A. J., and Cohen, R. C.: Differences in  
Regional Home Heating Behavior in Three U.S. Cities Revealed by Ground-Based Sensor Network, *Geophysical Research Letters*, 52,  
e2025GL115 772, <https://doi.org/10.1029/2025GL115772>, 2025.
- Bailey, D. M., Adkins, E. M., and Miller, J. H.: An Open-Path Tunable Diode Laser Absorption Spectrometer for Detection of Carbon Dioxide  
at the Bonanza Creek Long-Term Ecological Research Site near Fairbanks, Alaska, *Appl Phys B*, 123, 245, <https://doi.org/10.1007/s00340->  
265 017-6814-8, 2017.
- Birk, M., Röske, C., and Wagner, G.: The Pressure Dependence of the Experimentally-Determined Line Intensity and Contin-  
uum Absorption of Pure CO<sub>2</sub> in the 1.6 $\mu$ m Region, *Journal of Quantitative Spectroscopy and Radiative Transfer*, 324, 109 055,  
<https://doi.org/10.1016/j.jqsrt.2024.109055>, 2024a.
- Birk, M., Wagner, G., and Roeske, C.: Measurement and Line Parameter Database CO<sub>2</sub> 5975-6575 Cm<sup>-1</sup> Including Intensity Depletion and  
270 Continua, <https://doi.org/10.5281/ZENODO.10727028>, 2024b.
- Birk, M., Wagner, G., and Röske, C.: Absorption Cross Sections for Air- and H<sub>2</sub>O-broadened CO<sub>2</sub> in the 1.6  $\mu$ m and 2  $\mu$ m Regions (Including  
Continuum) and Air- and Self-Broadened H<sub>2</sub>O in the 1.6  $\mu$ m Region, <https://doi.org/10.5281/ZENODO.16746358>, 2025.
- Chen, X., Huang, C., Li, J., Lu, M., Li, Y., and Wei, H.: Phase-Sensitive Open-Path Dual-Comb Spectroscopy with Free-Running Combs,  
*Phys. Rev. Applied*, 19, 044 016, <https://doi.org/10.1103/PhysRevApplied.19.044016>, 2023.
- 275 Coburn, S., Alden, C. B., Wright, R., Cossel, K., Baumann, E., Truong, G.-W., Giorgetta, F., Sweeney, C., Newbury, N. R., Prasad, K.,  
Coddington, I., and Rieker, G. B.: Regional Trace-Gas Source Attribution Using a Field-Deployed Dual Frequency Comb Spectrometer,  
*Optica*, 5, 320, <https://doi.org/10.1364/OPTICA.5.000320>, 2018.
- Coddington, I., Newbury, N., and Swann, W.: Dual-Comb Spectroscopy, *OPTICA*, 3, 414, <https://doi.org/10.1364/OPTICA.3.000414>, 2016.
- Cole, R. K., Makowiecki, A. S., Hoghooghi, N., and Rieker, G. B.: Baseline-Free Quantitative Absorption Spectroscopy Based on Cepstral  
280 Analysis, *Opt. Express*, 27, 37 920, <https://doi.org/10.1364/OE.27.037920>, 2019.
- Cossel, K. C., Waxman, E. M., Giorgetta, F. R., Cermak, M., Coddington, I. R., Hesselius, D., Ruben, S., Swann, W. C., Truong,  
G.-W., Rieker, G. B., and Newbury, N. R.: Open-Path Dual-Comb Spectroscopy to an Airborne Retroreflector, *Optica*, 4, 724,  
<https://doi.org/10.1364/OPTICA.4.000724>, 2017.
- Cossel, K. C., Waxman, E. M., Baumann, E., Giorgetta, F. R., Coburn, S. C., Alden, C. B., and Washburn, B. R.: Remote Sens-  
285 ing Using Open-Path Dual-Comb Spectroscopy, in: *Advances in Spectroscopic Monitoring of the Atmosphere*, pp. 27–93, Elsevier,  
<https://doi.org/10.1016/B978-0-12-815014-6.00008-7>, 2021.
- Cossel, K. C., Waxman, E. M., Hoenig, E., Hesselius, D., Chaote, C., Coddington, I., and Newbury, N. R.: Ground-to-UAV, Laser-  
Based Emissions Quantification of Methane and Acetylene at Long Standoff Distances, *Atmos. Meas. Tech.*, 16, 5697–5707,  
<https://doi.org/10.5194/amt-16-5697-2023>, 2023.



- 290 Deutscher, N. M., Naylor, T. A., Caldow, C. G. R., McDougall, H. L., Carter, A. G., and Griffith, D. W. T.: Performance of an Open-Path near-Infrared Measurement System for Measurements of CO<sub>2</sub> and CH<sub>4</sub> during Extended Field Trials, *ATMOS MEAS TECH*, 14, 3119–3130, <https://doi.org/10.5194/amt-14-3119-2021>, 2021.
- Dobler, J., Braun, M., Blume, N., and Zaccheo, T.: A New Laser Based Approach for Measuring Atmospheric Greenhouse Gases, *REMOTE SENS-BASEL*, 5, 6284–6304, <https://doi.org/10.3390/rs5126284>, 2013.
- 295 Dobler, J. T., Zaccheo, T. S., Pernini, T. G., Blume, N., Broquet, G., Vogel, F., Ramonet, M., Braun, M., Staufer, J., Ciais, P., and Botos, C.: Demonstration of Spatial Greenhouse Gas Mapping Using Laser Absorption Spectrometers on Local Scales, *J. Appl. Remote Sens*, 11, 014 002, <https://doi.org/10.1117/1.JRS.11.014002>, 2017.
- Eber, A., Fürst, L., Siegrist, F., Kirchner, A., Tschofenig, B., Di Vora, R., Speletz, A., and Bernhardt, B.: Coherent Field Sensing of Nitrogen Dioxide, *Opt. Express*, 32, 6575, <https://doi.org/10.1364/OE.513523>, 2024.
- 300 Estruch, C., Curcoll, R., Morguí, J.-A., Segura-Barrero, R., Vidal, V., Badia, A., Ventura, S., Gilabert, J., and Villalba, G.: Exploring How the Heterogeneous Urban Landscape Influences CO<sub>2</sub> Concentrations: The Case Study of the Metropolitan Area of Barcelona, *Urban Forestry & Urban Greening*, 99, 128 438, <https://doi.org/10.1016/j.ufug.2024.128438>, 2024.
- Gately, C. K. and Hutyra, L. R.: Large Uncertainties in Urban-Scale Carbon Emissions, *Journal of Geophysical Research: Atmospheres*, 122, 11,242–11,260, <https://doi.org/10.1002/2017JD027359>, 2017.
- 305 Giorgetta, F. R., Peischl, J., Herman, D. I., Ycas, G., Coddington, I., Newbury, N. R., and Cossel, K. C.: Open-Path Dual-Comb Spectroscopy for Multispecies Trace Gas Detection in the 4.5–5 μm Spectral Region, *Laser & Photonics Reviews*, 15, 2000583, <https://doi.org/10.1002/lpor.202000583>, 2021.
- Gordon, I., Rothman, L., Hargreaves, R., Gomez, F., Bertin, T., Hill, C., Kochanov, R., Tan, Y., Wcisło, P., Makhnev, V. Yu., Bernath, P., Birk, M., Boudon, V., Campargue, A., Coustenis, A., Drouin, B., Gamache, R., Hodges, J., Jacquemart, D., Mlawer, E., Nikitin, A., Perevalov, V., 310 Rotger, M., Robert, S., Tennyson, J., Toon, G., Tran, H., Tyuterev, V., Adkins, E., Barbe, A., Bailey, D., Bielska, K., Bizzocchi, L., Blake, T., Bowesman, C., Cacciani, P., Čermák, P., Császár, A., Denis, L., Egbert, S., Egorov, O., Ermilov, A. Yu., Fleisher, A., Fleurbaey, H., Foltynowicz, A., Furtenbacher, T., Germann, M., Guest, E., Harrison, J., Hartmann, J.-M., Hjältén, A., Hu, S.-M., Huang, X., Johnson, T., Jóźwiak, H., Kassi, S., Khan, M., Kwabia-Tchana, F., Lee, T., Lisak, D., Liu, A.-W., Lyulin, O., Malarich, N., Manceron, L., Marinina, A., Massie, S., Mascio, J., Medvedev, E., Meshkov, V., Mellau, G. Ch., Melosso, M., Mikhailenko, S., Mondelain, D., Müller, H., O'Donnell, 315 M., Owens, A., Perrin, A., Polyansky, O., Raston, P., Reed, Z., Rey, M., Richard, C., Rieker, G., Röske, C., Sharpe, S., Starikova, E., Stolarczyk, N., Stolyarov, A., Sung, K., Tamassia, F., Terragni, J., Ushakov, V., Vasilchenko, S., Vispoel, B., Vodopyanov, K., Wagner, G., Wójtewicz, S., Yurchenko, S., and Zobov, N.: The HITRAN2024 Molecular Spectroscopic Database, *Journal of Quantitative Spectroscopy and Radiative Transfer*, 353, 109 807, <https://doi.org/10.1016/j.jqsrt.2026.109807>, 2026.
- Griffith, D. W. T., Pöhler, D., Schmitt, S., Hammer, S., Vardag, S. N., and Platt, U.: Long Open-Path Measurements of Greenhouse Gases in 320 Air Using near-Infrared Fourier Transform Spectroscopy, *ATMOS MEAS TECH*, 11, 1549–1563, <https://doi.org/10.5194/amt-11-1549-2018>, 2018.
- Gurney, K. R., Liang, J., Roest, G., Song, Y., Mueller, K., and Lauvaux, T.: Under-Reporting of Greenhouse Gas Emissions in U.S. Cities, *NAT COMMUN*, 12, 553, <https://doi.org/10.1038/s41467-020-20871-0>, 2021.
- Han, J.-J., Zhong, W., Zhao, R.-C., Zeng, T., Li, M., Lu, J., Peng, X.-X., Shi, X.-P., Yin, Q., Wang, Y., Esamdin, A., Shen, Q., Guan, J.-Y., 325 Hou, L., Ren, J.-G., Jia, J.-J., Wang, Y., Jiang, H.-F., Xue, X.-H., Zhang, Q., Dou, X.-K., and Pan, J.-W.: Dual-Comb Spectroscopy over a 100 Km Open-Air Path, *Nat. Photon.*, 18, 1195–1202, <https://doi.org/10.1038/s41566-024-01525-9>, 2024.



- Herman, D. I., Weerasekara, C., Hutcherson, L. C., Giorgetta, F. R., Cossel, K. C., Waxman, E. M., Colacion, G. M., Newbury, N. R., Welch, S. M., DePaola, B. D., Coddington, I., Santos, E. A., and Washburn, B. R.: Precise Multispecies Agricultural Gas Flux Determined Using Broadband Open-Path Dual-Comb Spectroscopy, *Sci. Adv.*, 7, eabe9765, <https://doi.org/10.1126/sciadv.abe9765>, 2021.
- 330 Hong, S.-O., Kim, J., Byun, Y.-H., Hong, J., Hong, J.-W., Lee, K., Park, Y.-S., Lee, S.-S., and Kim, Y.-H.: Intra-Urban Variations of the CO<sub>2</sub> Fluxes at the Surface-Atmosphere Interface in the Seoul Metropolitan Area, *Asia-Pac J Atmos Sci*, 59, 417–431, <https://doi.org/10.1007/s13143-023-00324-6>, 2023.
- Kaminski, T., Rayner, P. J., Heimann, M., and Enting, I. G.: On Aggregation Errors in Atmospheric Transport Inversions, *J. Geophys. Res.*, 106, 4703–4715, <https://doi.org/10.1029/2000JD900581>, 2001.
- 335 Kim, J., Berelson, W. M., Rollins, N. E., Asimow, N. G., Newman, C., Cohen, R. C., Miller, J. B., McDonald, B. C., Peischl, J., and Lehman, S. J.: Observing Anthropogenic and Biogenic CO<sub>2</sub> Emissions in Los Angeles Using a Dense Sensor Network, *Environ. Sci. Technol.*, 59, 3508–3517, <https://doi.org/10.1021/acs.est.4c11392>, 2025.
- Kochanov, R., Gordon, I., Rothman, L., Wcislo, P., Hill, C., and Wilzewski, J.: HITRAN Application Programming Interface (HAPI): A Comprehensive Approach to Working with Spectroscopic Data, *J QUANT SPECTROSC RA*, 177, 15–30, <https://doi.org/10.1016/j.jqsrt.2016.03.005>, 2016.
- 340 Lauvaux, T., Gurney, K. R., Miles, N. L., Davis, K. J., Richardson, S. J., Deng, A., Nathan, B. J., Oda, T., Wang, J. A., Hutyra, L., and Turnbull, J.: Policy-Relevant Assessment of Urban CO<sub>2</sub> Emissions, *Environ. Sci. Technol.*, 54, 10237–10245, <https://doi.org/10.1021/acs.est.0c00343>, 2020.
- Lian, J., Bréon, F.-M., Broquet, G., Zaccheo, T. S., Dobler, J., Ramonet, M., Staufer, J., Santaren, D., Xueref-Remy, I., and Ciais, P.: Analysis of Temporal and Spatial Variability of Atmospheric CO<sub>2</sub> Concentration within Paris from the GreenLITE™ Laser Imaging Experiment, *ATMOS CHEM PHYS*, 19, 13 809–13 825, <https://doi.org/10.5194/acp-19-13809-2019>, 2019.
- Malarich, N., Giorgetta, F. R., Mead, G., Baumann, E., Genest, J., Newbury, N. R., Coddington, I., and Cossel, K. C.: Evaluating CO<sub>2</sub> and CH<sub>4</sub> Absorption Models with Open-Path Dual-Comb Spectroscopy at the Mauna Loa Observatory, *Journal of Quantitative Spectroscopy and Radiative Transfer*, 345, 109 567, <https://doi.org/10.1016/j.jqsrt.2025.109567>, 2025.
- 350 Mead, G. J., Waxman, E. M., Bon, D., Herman, D. I., Baumann, E., Giorgetta, F. R., Friedlein, J. T., Ycas, G., Newbury, N. R., Coddington, I., and Cossel, K. C.: Open-Path Dual-Comb Spectroscopy of Methane and VOC Emissions from an Unconventional Oil Well Development in Northern Colorado, *Front. Chem.*, 11, 1202 255, <https://doi.org/10.3389/fchem.2023.1202255>, 2023.
- Mitchell, L. E., Lin, J. C., Bowling, D. R., Pataki, D. E., Strong, C., Schauer, A. J., Bares, R., Bush, S. E., Stephens, B. B., Mendoza, D., Mallia, D., Holland, L., Gurney, K. R., and Ehleringer, J. R.: Long-Term Urban Carbon Dioxide Observations Reveal Spatial and Temporal Dynamics Related to Urban Characteristics and Growth, *Proceedings of the National Academy of Sciences*, 115, 2912–2917, <https://doi.org/10.1073/pnas.1702393115>, 2018.
- 355 Mueller, K. L., Lauvaux, T., Gurney, K. R., Roest, G., Ghosh, S., Gourdj, S. M., Karion, A., DeCola, P., and Whetstone, J.: An Emerging GHG Estimation Approach Can Help Cities Achieve Their Climate and Sustainability Goals, *ENVIRON RES LETT*, 16, 084 003, <https://doi.org/10.1088/1748-9326/ac0f25>, 2021.
- 360 Oda, T., Bun, R., Kinakh, V., Topylko, P., Halushchak, M., Marland, G., Lauvaux, T., Jonas, M., Maksyutov, S., Nahorski, Z., Lesiv, M., Danylo, O., and Horabik-Pyzel, J.: Errors and Uncertainties in a Gridded Carbon Dioxide Emissions Inventory, *Mitig Adapt Strateg Glob Change*, 24, 1007–1050, <https://doi.org/10.1007/s11027-019-09877-2>, 2019.
- Park, C., Jeong, S., Park, M.-S., Park, H., Yun, J., Lee, S.-S., and Park, S.-H.: Spatiotemporal Variations in Urban CO<sub>2</sub> Flux with Land-Use Types in Seoul, *Carbon Balance Manage*, 17, 3, <https://doi.org/10.1186/s13021-022-00206-w>, 2022.



- 365 Patel, M. Y., Asimow, N. G., Winter, A. R., Zhu, Y., and Cohen, R. C.: Using Network Observations to Constrain CO and CO<sub>2</sub> Emissions From an Oil Refinery in the San Francisco Bay Area, *Journal of Geophysical Research: Atmospheres*, 131, e2025JD045 035, <https://doi.org/10.1029/2025JD045035>, 2026.
- Picqué, N. and Hänsch, T. W.: Frequency Comb Spectroscopy, *Nature Photon*, 13, 146–157, <https://doi.org/10.1038/s41566-018-0347-5>, 2019.
- 370 Plant, G., Nikodem, M., Mulhall, P., Varner, R., Sonnenfroh, D., and Wysocki, G.: Field Test of a Remote Multi-Path CLaDS Methane Sensor, *Sensors*, 15, 21 315–21 326, <https://doi.org/10.3390/s150921315>, 2015.
- Quatrevalet, M., Wolferstetter, M., Sprenger, B., Fischer, M., Holzwarth, R., and Fix, A.: In-Flight Enhancement of the Optical Frequency Accuracy of an Integral-Path Differential Absorption Lidar Thanks to a Rugged, Airborne Self-Referenced Frequency Comb, *Opt. Express*, 33, 10 165, <https://doi.org/10.1364/OE.546616>, 2025.
- 375 Rieker, G. B., Giorgetta, F. R., Swann, W. C., Kofler, J., Zolot, A. M., Sinclair, L. C., Baumann, E., Cromer, C., Petron, G., Sweeney, C., Tans, P. P., Coddington, I., and Newbury, N. R.: Frequency-Comb-Based Remote Sensing of Greenhouse Gases over Kilometer Air Paths, *Optica*, 1, 290, <https://doi.org/10.1364/OPTICA.1.000290>, 2014.
- Saito, H., Manago, N., Kuriyama, K., and Kuze, H.: Near-Infrared Open-Path Measurement of CO<sub>2</sub> Concentration in the Urban Atmosphere, *Opt. Lett.*, 40, 2568, <https://doi.org/10.1364/OL.40.002568>, 2015.
- 380 Schmitt, T. D., Kuhn, J., Kleinschek, R., Löw, B. A., Schmitt, S., Cranton, W., Schmidt, M., Vardag, S. N., Hase, F., Griffith, D. W. T., and Butz, A.: An Open-Path Observatory for Greenhouse Gases Based on near-Infrared Fourier Transform Spectroscopy, *Atmospheric Measurement Techniques*, 16, 6097–6110, <https://doi.org/10.5194/amt-16-6097-2023>, 2023.
- Shusterman, A. A., Teige, V. E., Turner, A. J., Newman, C., Kim, J., and Cohen, R. C.: The Berkeley Atmospheric CO<sub>2</sub> Observation Network: Initial Evaluation, *ATMOS CHEM PHYS*, 16, 13 449–13 463, <https://doi.org/10.5194/acp-16-13449-2016>, 2016.
- 385 Super, I., Dellaert, S. N. C., Visschedijk, A. J. H., and Denier Van Der Gon, H. A. C.: Uncertainty Analysis of a European High-Resolution Emission Inventory of CO<sub>2</sub> and CO to Support Inverse Modelling and Network Design, *Atmos. Chem. Phys.*, 20, 1795–1816, <https://doi.org/10.5194/acp-20-1795-2020>, 2020.
- Truong, G.-W., Waxman, E. M., Cossel, K. C., Baumann, E., Klose, A., Giorgetta, F. R., Swann, W. C., Newbury, N. R., and Coddington, I.: Accurate Frequency Referencing for Fieldable Dual-Comb Spectroscopy, *OPT EXPRESS*, 24, 30495, <https://doi.org/10.1364/OE.24.030495>, 2016.
- 390 Waxman, E. M., Cossel, K. C., Truong, G.-W., Giorgetta, F. R., Swann, W. C., Coburn, S., Wright, R. J., Rieker, G. B., Coddington, I., and Newbury, N. R.: Intercomparison of Open-Path Trace Gas Measurements with Two Dual-Frequency-Comb Spectrometers, *ATMOS MEAS TECH*, 10, 3295–3311, <https://doi.org/10.5194/amt-10-3295-2017>, 2017.
- Waxman, E. M., Cossel, K. C., Giorgetta, F., Truong, G.-W., Swann, W. C., Coddington, I., and Newbury, N. R.: Estimating Vehicle Carbon Dioxide Emissions from Boulder, Colorado, Using Horizontal Path-Integrated Column Measurements, *ATMOS CHEM PHYS*, 19, 4177–4192, <https://doi.org/10.5194/acp-19-4177-2019>, 2019.
- Zaccheo, T. S., Blume, N., Pernini, T., Dobler, J., and Lian, J.: Bias Correction of Long-Path CO<sub>2</sub> Observations in a Complex Urban Environment for Carbon Cycle Model Inter-Comparison and Data Assimilation, *Atmos. Meas. Tech.*, 12, 5791–5800, <https://doi.org/10.5194/amt-12-5791-2019>, 2019.
- 400 Zhu, X.-H., Lu, K.-F., Peng, Z.-R., He, H.-D., and Xu, S.-Q.: Spatiotemporal Variations of Carbon Dioxide (CO<sub>2</sub>) at Urban Neighborhood Scale: Characterization of Distribution Patterns and Contributions of Emission Sources, *Sustainable Cities and Society*, 78, 103 646, <https://doi.org/10.1016/j.scs.2021.103646>, 2022.